

Research on Thermal Analysis and Optimization of a Certain Type of Antenna Orbit Based on NX TMG and HFSS Co-Simulation

Liang Hu^{1,2,a}, Hongbin Zhao^{1,2,b}, Huyong Zhang^{1,2,c}, Hongchao Li^{1,2,d}

¹ The 39th Research Institute of China Electronics Technology Group Corporation, Xi'an, 710065;

² Shaanxi Key Laboratory of Antenna and Control Technology, Xi'an, 710065

^a feiyu123451001@sina.com, ^b zyx95@sina.com.cn, ^c zhanghuyong@163.com,

^d 516073295@qq.com

Abstract. Antennas on satellites in orbit must withstand periodic and non-uniform thermal environments, which directly affect the quality of satellite communication. Given known satellite orbit parameters and attitude, a finite element model of the antenna temperature field is established using NX TMG software to calculate the transient temperature field of the antenna in orbit. Thermal control modeling is performed on areas of the antenna that experience high or low temperatures, and through iterative optimization, Determine the thermal control plan for antennas. Subsequently, the temperature field is applied to the antenna structure's finite element model, and the thermal deformation of the antenna is obtained using NX Nastran. The deformed antenna model is then imported into HFSS software to solve for changes in electrical performance indicators, thereby determining whether the antenna can function normally under the conditions of an in-orbit, non-uniform temperature field.

Keywords : Antenna; Orbital Thermal Analysis; Thermal Deformation; Electrical Performance; Thermal Control

1. Introduction

The working environment of satellites in orbit is the cosmic space outside the Earth's atmosphere, where heat exchange with the space environment mainly relies on radiation and conduction. The surface facing the Sun may experience temperatures above 100°C, while the surface away from the Sun has to contend with a cold environment of -269°C (3K). As the satellite's position relative to the Sun and Earth continuously changes, the amount of external heat it receives also undergoes drastic variations [1].

Severe temperature fluctuations can cause materials to age rapidly, significantly reducing their service life. High temperatures can decrease the strength of structural materials, affecting the overall stability of structures; low temperatures, on the other hand, can make materials brittle, which in severe cases can lead to structural failure [2][3]. Depending on the different characteristics and requirements of the equipment on the satellite, all are required to operate within a certain temperature range to ensure their performance. Antennas, as key payloads of satellites, are mounted on the surface of the satellite body and experience a harsher space environment than the internal equipment. Frequent drastic temperature changes form thermal shocks that affect antenna structural deformation, which can greatly impact the electrical performance of the antenna [4][5]. Therefore, it is essential to perform thermal analysis and design for antennas in orbit.

Since the space environment is a high vacuum, the heat exchange between antennas and satellites, as well as with space, is mainly conducted through radiation and conduction. The expression for the thermal balance relationship of the antenna in space is as follows:

$$q_1 + q_2 + q_3 + q_4 = q_5 + q_6$$

In this equation:

q_1 — represents the solar direct radiation power rate.

q_2 — represents the earth-reflected radiation power rate.

q_3 —represents the earth's infrared radiation power rate.

q_4 —represents the heat conduction power rate between the satellite and the antenna.

q_5 —represents the rate of internal energy change within the antenna.

q_6 —represents the radiation power rate of the antenna to the cosmic space.

q_5 , which is the rate of internal energy change in the antenna, macroscopically manifests as a change in the object's temperature, leading to thermal stress and deformation due to temperature changes. Compared with general stress analysis problems, considering the physical equation for thermal stress:

$$\{\sigma\} = [D](\{\epsilon\} - \{\epsilon_0\})$$

where: $\{\sigma\}$ is the stress induced by temperature,

$\{\epsilon_0\}$ is the deformation,

$[D]$ is the material's modulus of elasticity.

And for the thermal strain-temperature relationship:

$$\{\epsilon_0\} = \alpha T[1 \ 1 \ 1 \ 1 \ 1 \ 1]T$$

In this equation: α is the coefficient of thermal expansion of the material,

T is the temperature change.

This paper uses NX TMG software to perform orbital thermal analysis on a certain type of satellite antenna, obtaining the transient temperature field in orbit. Then, the temperature field is applied as a thermal load to the structural finite element model to calculate structural thermal deformation. The deformed structural model is then input into HFSS software in the form of digital modeling to analyze changes in the electrical performance of the antenna. At the same time, passive or active thermal control modeling is conducted for locations with drastic temperature changes. Through iterative optimization, a feasible thermal control scheme is confirmed, providing a basis for the thermal design of the antenna.

2. Satellite Antenna Thermal Simulation Model

2.1 Antenna Structure

The three-dimensional model of a certain type of antenna structure for simulation analysis is shown in Figure 1.

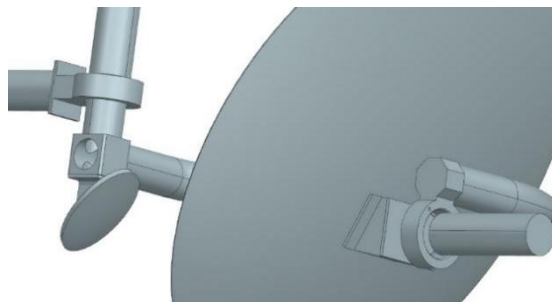


Fig.1 Illustration of the Antenna Three-Dimensional Model

This antenna mainly consists of the main reflector, sub-reflector, support structure, and motors a and b. The antenna product is installed on the satellite's side plate, and the main reflector adjusts its spatial attitude under the action of motors a and b.

2.2 Material Parameters

Both the main reflector and sub-reflector are made of aluminum alloy, the main reflector support structure and sub-reflector support structure rods are primarily made of carbon fiber material, the upper and lower flanges of the support structure are made of titanium alloy, and the outer shells of motors a and b are also made of titanium alloy. The satellite cabin plate and solar wing sail board surfaces are all made of carbon fiber material.

For thermal analysis, the absorption rate and emissivity of materials are two essential thermo-optical property parameters. The physical properties of the materials are shown in Table 1.

Table 1 Material Physical Properties

Unit: density/ kg/m^3 ;

Thermal expansion coefficient/ $1/^\circ\text{C}$;

Thermal conductivity/ W/m.K

Specific heat/ $\text{J/Kg.}^\circ\text{C}$

| Material | Density | Thermal expansion Factor | Thermal conductivity | Specific heat | Emissivity | Absorption rate |
|----------------|---------|--------------------------|----------------------|---------------|------------|-----------------|
| Titanium alloy | 4430 | $7.9\text{e-}6$ | 8.8 | 550 | 0.63 | 0.45 |
| Aluminum alloy | 2780 | $23.6\text{e-}6$ | 117.2 | 921 | 0.24 | 0.14 |
| Polyimide | 1450 | $2.5\text{e-}5$ | 0.32 | 175 | 0.84 | 0.53 |
| Carbon fiber | 1620 | $1.2\text{e-}6$ | 0.42 | 596 | 0.86 | 0.85 |

2.3 Boundary Conditions Setting

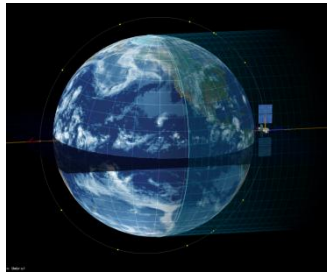


Fig.2 illustrates the satellite's orbit

The satellite flies in a near-polar sun-synchronous orbit, with its flight simulation image shown in Figure 2. The orbit's inclination is close to 90° , and the average altitude is 1200 km. Satellite attitude parameters: -Z axis always points to Earth.

Considering that the antenna is unpowered and has no thermal dissipation, the thermal field boundary considers solar radiation, radiation from the satellite body to the antenna, and contact between antenna components.

2.4 Mesh Division

Ignoring the influence of other satellite equipment on the thermal field of the analyzed antenna, only considering the influence of the satellite body and solar wings on the analyzed antenna, simplifying the satellite body, solar wings, and antenna structure, using NX TMG software for mesh division and establishing an assembly finite element model, as shown in Figure 3.

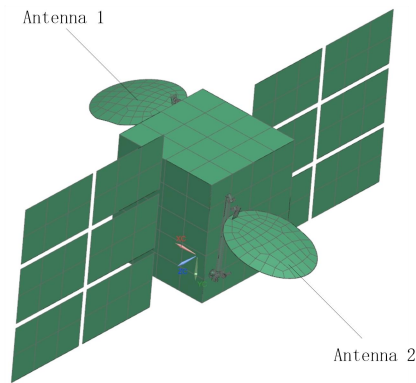


Fig.3 Satellite Antenna Mesh Model

To reduce the size of the finite element analysis unit and shorten the analysis calculation time, the model uses shell elements, with larger mesh sizes for the satellite body and solar wings; smaller mesh sizes are used for critical antenna components (such as the main reflector and sub-reflector) to improve calculation accuracy.

2.5 Orbital Thermal Simulation Results

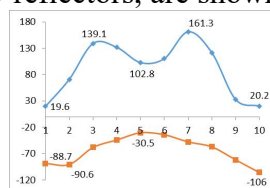
2.5.1 Thermal Control Iterative Optimization Results

After preliminary simulation calculations, extracting the transient temperature field at 10 points on the complete orbit surface, it was found that the temperature change of the support rods (thin-walled structure) was severe. The highest and lowest temperature points of the entire antenna were both located on the thin-walled rods, and their temperature changes affected the connected motors, main reflector, and sub-reflector through thermal conduction, causing the motors to exceed the normal working temperature (not higher than 50°C), and the temperature difference on the main and sub-reflectors became larger, resulting in significant thermal deformation. After multiple thermal control optimizations, the following thermal treatment options were determined for local antenna components:

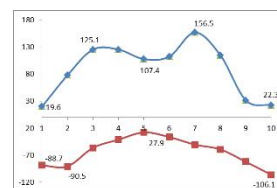
- (1) Install a 5mm thick thermal pad between motor a and its corresponding mount, between motor b and its corresponding mount, and between the main reflector and its corresponding mount. The thermal pad is made of polyimide material;
- (2) Spray white paint on the back of the main reflector;
- (3) Add light shields to both motor a and motor b, which are made of polyimide material with a thickness of 2mm and a gap of 2mm from the motors;
- (4) The surface of the carbon fiber material on the main and sub-reflector support structure rods is covered with multiple layers.

2.5.2 Antenna Thermal Field Simulation Results

Based on the above thermal control measures, the antenna model was modified accordingly, and the transient temperature field at 10 points on the complete orbit surface was extracted again, obtaining the temperature change curves of antenna 1 and antenna 2, as shown in Figure 4; at the same time, the temperature change situation of each component, the temperature change curves of the main and sub-reflectors, are shown in Figure 5.

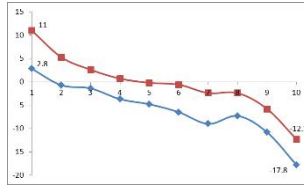


(A) Overall temperature change curve of Antenna 1

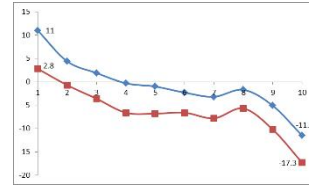


(B) Overall temperature change curve of Antenna 2

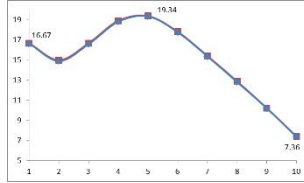
Fig.4 Overall Temperature Change Curve of the Antenna



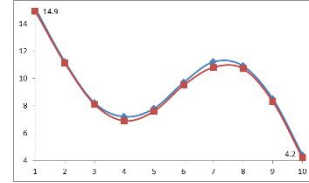
(A) Main reflector temperature change curve of Antenna 1



(B) Main reflector temperature change curve of Antenna 2



(C) Sub-reflector temperature change curve of Antenna 1



(D) Sub-reflector temperature change curve of Antenna 2

Fig.5 Main and Sub-Reflector Temperature Change Curves

Antennas 1 and 2 are located on both sides of the satellite X-axis and are both mounted facing Earth. From the overall temperature change curves of antennas 1 and 2, the temperature change trends of the two antennas are consistent, which is in line with objective conditions. The highest temperature point of the antenna is located at increment 15 (1307s), and the lowest temperature point is located at increment 23 (6535.2s).

Analyzing the overall temperature cloud diagram of the antenna, the highest temperature point of the antenna is located on the sub-reflector support structure (thin-walled rod), and the lowest temperature point of the antenna is located on the motor b light shield. The highest and lowest temperature points of the two sub-antennas occur at the same position. As can be seen from Figure 5, the temperature change trends of the main and sub-reflectors of the antenna are similar; the maximum temperature difference of the main reflector is 8.2°C, and the sub-reflector temperature is uniform, indicating that spraying white paint on the back of the main reflector and installing thermal pads can reduce local thermal conduction and ensure temperature uniformity of the reflector. The temperature change range of the antenna motor and motor light shield is shown in Table 2.

Table 2 Temperature Variations of Antenna Motors and Motor Sunshades

| | Motor A | Motor A Sunshade | Motor B | Motor B Sunshade |
|-----------|-------------------|-------------------|------------------|--------------------|
| Antenna 1 | +14.4°C ~ +25.5°C | -77.2°C ~ +71.9°C | +1.8°C ~ +19.6°C | -106°C ~ +72°C |
| Antenna 2 | +11.7°C ~ +27.7°C | -78.3°C ~ +76.9°C | +1.2°C ~ +19.6°C | -106.1°C ~ +71.6°C |

From Table 2, it can be observed that after the installation of light shields on motors a and b of both antennas, the temperature variation was significantly suppressed, meeting the normal operating temperature requirements of the motors; from the range of temperature changes in the motors and light shields, it is evident that the light shields played a significant "insulation" role for the motors.

3. Antenna Structural Finite Element Model

3.1 Establishment of the Structural Finite Element Model

The simplified star body, solar panels, and antenna structures were meshed and an assembly finite element model was established. The model used shell elements throughout; the star body and solar panel parts, which are not under assessment, continued to use larger mesh sizes; whereas the antenna used smaller mesh sizes to improve calculation precision. RBE2 rigid elements were used to connect between the star body and solar panels, the antenna and the star body, and various connected parts of the antenna.

3.2 Definition of Material and Boundary Conditions

Material parameters were assigned to different parts of the antenna. The material structural performance parameters are shown in Table 3.

Table 3 Material Structural Performance Parameters

Unit: Density / kg/m³
Elastic Modulus / MPa
Allowable Stress / MPa

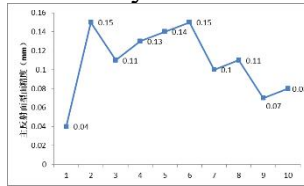
| Material | Density | Modulus of elasticity | Poisson's ratio | Allowable stress |
|-------------------------------------|---------|-----------------------|-----------------|------------------|
| Titanium Alloy | 4430 | 113000 | 0.3 | 815 |
| Aluminum Alloy (Bright Anodized) | 2780 | 70000 | 0.3 | 238 |
| Polyimide | 1450 | 2000 | 0.35 | 100 |
| Carbon fiber | 1620 | 120000 | 0.3 | 600 |

The temperature field was loaded as a thermal load onto the structural finite element model.

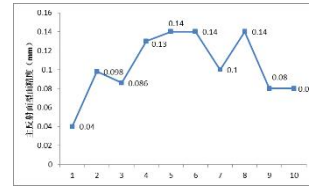
3.3 Antenna Thermal Deformation Simulation Results

Surface accuracy is a key indicator for reflector antennas, affecting the radiation pattern and thereby the gain and directivity of the antenna. Higher surface accuracy results in a radiation pattern closer to the ideal state, leading to better gain and directivity of the antenna, as well as lower reflection losses of electromagnetic waves.

The NX Nastran software was used to solve the structural finite element model, extracting the displacement of all nodes on the main reflector and calculating the standard deviation of displacement along the Z-axis to obtain the surface accuracy of the antenna's main reflector. The change in surface accuracy of the antenna is shown in Figure 6.



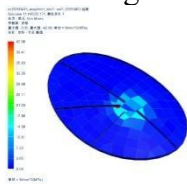
(A) Surface accuracy of Antenna 1 main reflector



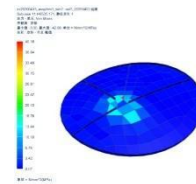
(B) Surface accuracy of Antenna 2 main reflector

Fig.6 Change in Antenna Surface Accuracy

As seen from Figure 7, the surface accuracies of the main reflectors of Antennas 1 and 2 are 0.15mm and 0.14mm, respectively, meeting the related indicator requirements for surface accuracy. The stress on the main reflectors of Antennas 1 and 2 was extracted, and the thermal stress nephogram is shown in Figure 7.



(A) Max stress nephogram of Antenna 1 main reflector



(B) Max stress nephogram of Antenna 2 main reflector

Fig.7 Main Reflector Thermal Stress Nephogram

The maximum stress on the main reflector occurred at increment 23 (6535.2s), with Antenna 1's main reflector reaching a maximum stress of 43MPa and Antenna 2's main reflector reaching a maximum stress of 40.2MPa, both occurring at the connection surface of the main reflector. Since the main reflector material is aluminum alloy, the material stress meets the strength margin requirements.

4. Antenna Electrical Performance Review

The HFSS software was used to establish an electrical model of the antenna, as shown in Figure 8. The electrical model mainly consists of the main reflector, sub-reflector, and feed horn. During modeling, the Z-axis of the coordinate system coincided with the axis of rotational symmetry of the main reflector, meaning the maximum radiation direction of the antenna was along the positive Z-axis. Before thermal deformation occurred, the reflector was ideal, and the electrical performance of Antennas 1 and 2 was consistent, with their gain directional diagram simulation results shown in Figure 9. At this time, the maximum radiation direction of Antennas 1 and 2 was along the positive Z-axis.

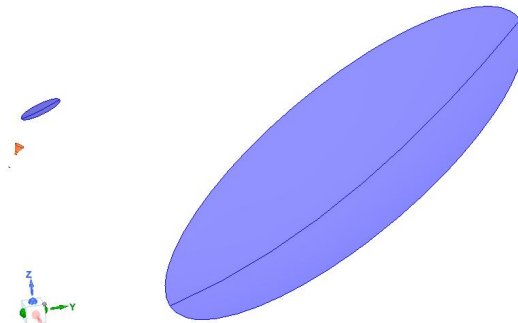


Fig.8 Modeling of Antennas 1 and 2 in HFSS

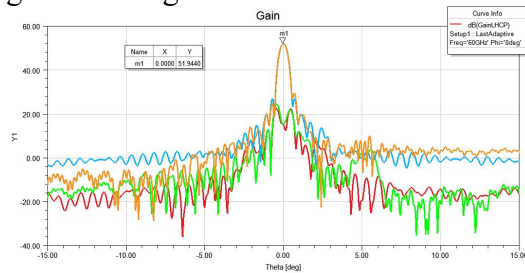


Fig.9 Gain Directional Diagram Simulation Results for Antennas 1 and 2 with No Thermal Deformation

Before thermal control measures were implemented, according to the gain directional diagram simulation results modeled in HFSS after thermal deformation of Antennas 1 and 2, as shown in Figure 10, Antenna 1's gain decreased by 1dB, and the maximum radiation direction deviated by 0.05° from the Z-axis. Antenna 2's gain decreased by 1.13dB, and the maximum radiation direction deviated by 0.06° from the Z-axis.

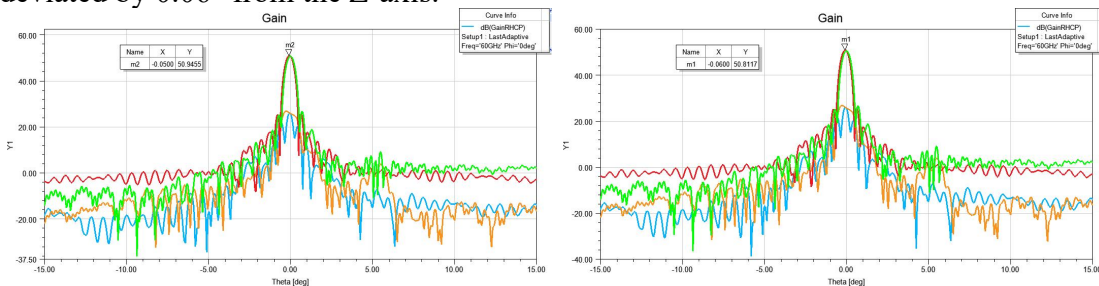


Fig.10 Gain Directional Diagram Simulation Results for Antennas 1 and 2 Without Thermal Control, After Thermal Deformation Occurred

After thermal control optimization, according to the gain directional diagram simulation results modeled in HFSS after thermal deformation of Antennas 1 and 2, as shown in Figure 11, Antenna 1's gain decreased by 0.41dB, and Antenna 2's gain decreased by 0.47dB. The maximum radiation directions of Antennas 1 and 2 were along the Z-axis.

